



First decay-time-dependent analysis of $B^0 \rightarrow K^0 \pi^0$ decays at Belle II

(Belle II Collaboration)

Abstract

We report measurements of the branching fraction (\mathcal{B}) and direct CP -violating asymmetry (\mathcal{A}_{CP}) of the charmless decay $B^0 \rightarrow K^0 \pi^0$ at Belle II. A sample of e^+e^- collisions, corresponding to 189.8 fb^{-1} of integrated luminosity, recorded at the $\Upsilon(4S)$ resonance is used for the first Belle II decay-time-dependent analysis of these decays. We reconstruct about 135 signal candidates, and measure $\mathcal{B}(B^0 \rightarrow K^0 \pi^0) = [11.0 \pm 1.2(\text{stat}) \pm 1.0(\text{syst})] \times 10^{-6}$ and $\mathcal{A}_{CP}(B^0 \rightarrow K^0 \pi^0) = -0.41_{-0.32}^{+0.30}(\text{stat}) \pm 0.08(\text{syst})$.

16 **1. INTRODUCTION**

17 The $B^0 \rightarrow K^0 \pi^0$ decay is mediated by flavour-changing neutral currents. In the standard
 18 model (SM), the dominant decay amplitude is given by the $b \rightarrow s \bar{d} \bar{d}$ loop, which is dominated
 19 by the top quark contribution and carries a weak phase $\arg(V_{tb} V_{ts}^*)$. Here, V_{ij} denote the
 20 CKM matrix elements. Such processes are suppressed in the SM and provide an indirect
 21 route to search for beyond-the-SM particles that might be exchanged in the loop. In the
 22 $B^0 \rightarrow K^0 \pi^0$ decay, CP violation can occur either directly in the decay amplitude (\mathcal{A}_{CP})
 23 or via the interference between decays with and without $B^0-\bar{B}^0$ mixing (\mathcal{S}_{CP}). Neglecting
 24 subleading contributions to the amplitude, \mathcal{S}_{CP} is expected to be equal to $\sin 2\phi_1$ and $\mathcal{A}_{CP} \approx$
 25 0, where $\phi_1 \equiv \arg(-V_{cd} V_{cb}^*/V_{td} V_{tb}^*)$. Deviations from these expectations could be due to
 26 larger-than-expected subleading SM contributions or by non-SM physics.

27 Combining B -meson lifetimes (τ) with branching fractions (\mathcal{B}) and CP asymmetries of
 28 four $B \rightarrow K \pi$ decays related by isospin symmetry, the proposed sum rule,

$$\begin{aligned}
 I_{K\pi} = & \mathcal{A}_{CP}(K^+ \pi^-) + \mathcal{A}_{CP}(K^0 \pi^+) \frac{\mathcal{B}(K^0 \pi^+) \tau_{B^0}}{\mathcal{B}(K^+ \pi^-) \tau_{B^+}} & (1) \\
 & - 2\mathcal{A}_{CP}(K^+ \pi^0) \frac{\mathcal{B}(K^+ \pi^0) \tau_{B^0}}{\mathcal{B}(K^+ \pi^-) \tau_{B^+}} - 2\mathcal{A}_{CP}(K^0 \pi^0) \frac{\mathcal{B}(K^0 \pi^0)}{\mathcal{B}(K^+ \pi^-)} = 0,
 \end{aligned}$$

29 is expected to hold with an uncertainty below 1% and provides an important consistency
 30 test of the SM [3]. Deviations from the isospin sum rule can be caused by an enhancement of
 31 color-suppressed tree amplitudes, or by contributions from non-SM physics. The value of $I_{K\pi}$
 32 has been measured to be 0.03 ± 0.08 [4]. The dominant uncertainty on $I_{K\pi}$ sensitivity comes
 33 from the uncertainty of $\mathcal{A}_{CP}(K^0 \pi^0)$. Combining measurements from Belle and BaBar [1,
 34 2], particle data group find $\mathcal{A}_{CP}(B^0 \rightarrow K^0 \pi^0) = 0.00 \pm 0.13$ [5]. Therefore a precise
 35 measurement of $\mathcal{A}_{CP}(K^0 \pi^0)$ is very important for the consistency test of SM.

36 Preliminary results on \mathcal{B} and \mathcal{A}_{CP} of $B^0 \rightarrow K^0 \pi^0$ decays have been reported by Belle II
 37 using a data sample corresponding to 62.8 fb^{-1} . In this analysis, we utilize a larger data set
 38 (189.8 fb^{-1}) and further enhance our sensitivity to \mathcal{A}_{CP} by using B decay time information.

39 At Belle II, pairs of neutral B mesons are coherently produced in the process $e^+ e^- \rightarrow$
 40 $\Upsilon(4S) \rightarrow B^0 \bar{B}^0$. When one of the B mesons decays to a CP eigenstate f_{CP} , such as $K_s^0 \pi^0$,
 41 and the other to a flavor-specific final state f_{tag} , the time-dependent decay rate is given by

$$\mathcal{P}(\Delta t) = \frac{e^{-|\Delta t|/\tau_{B^0}}}{4\tau_{B^0}} [1 + q\{\mathcal{A}_{CP} \cos(\Delta m_d \Delta t) + \mathcal{S}_{CP} \sin(\Delta m_d \Delta t)\}], \quad (2)$$

42 where $\Delta t = t_{CP} - t_{\text{tag}}$ is the proper-time difference between the decays into f_{CP} and f_{tag} , q
 43 equals +1 (−1) for the B^0 (\bar{B}^0) decay to f_{tag} , and Δm_d is the $B^0-\bar{B}^0$ mixing frequency. This
 44 analysis employs a decay-time-dependent CP violation fit similar to previous measurements
 45 of $\sin 2\phi_1$ [6]. The key challenge for this analysis is to determine the position of the $B^0 \rightarrow$
 46 $K^0 \pi^0$ decay vertex. For that, the K_s^0 flight direction is projected back to the interaction
 47 region and the K_s^0 is required to decay inside the vertex detector. The full analysis had been
 48 developed and tested with simulated data, and validated with data control samples before
 49 selecting and inspecting the $B^0 \rightarrow K^0 \pi^0$ candidates. Due to the limited sensitivity provided
 50 by the available data sample, we measure \mathcal{A}_{CP} by fixing \mathcal{S}_{CP} , Δm_d and τ_{B^0} to their known
 51 values [7].

52 2. THE BELLE II DETECTOR AND DATA SAMPLE

53 Belle II [8] is a particle spectrometer having almost 4π solid-angle coverage, designed to
54 reconstruct final-state particles of e^+e^- collisions delivered by the SuperKEKB asymmetric-
55 energy collider [9]. It is located at the KEK laboratory in Tsukuba, Japan. The energies of
56 the positron and electron beams are 4 and 7 GeV, respectively. Belle II comprises a number
57 of subdetectors surrounding the interaction region in a cylindrical geometry. The innermost
58 one is the vertex detector (VXD), comprised of position-sensitive silicon sensors. It samples
59 the trajectories of charged particles (‘tracks’) in the vicinity of the interaction region to
60 determine the decay positions of their parent particles. The VXD includes two inner layers
61 of pixel sensors and four outer layers of double-sided microstrip sensors. The second pixel
62 layer is currently incomplete covering one sixth of the azimuthal angle. Charged-particle mo-
63 menta and charges are measured by a large-radius, small-cell, central drift chamber (CDC),
64 which also offers particle-identification information via a measurement of specific ionization.
65 A Cherenkov-light angle and time-of-propagation detector surrounding the CDC provides
66 charged-particle identification in the central detector volume, supplemented by proximity-
67 focusing, aerogel, ring-imaging Cherenkov detectors in the forward region with respect to
68 the electron beam. A CsI(Tl)-crystal electromagnetic calorimeter (ECL) provides energy
69 measurements of electrons and photons. A solenoid surrounding the ECL generates a uni-
70 form axial 1.5 T magnetic field. Layers of plastic scintillators and resistive-plate chambers,
71 interspersed between the magnetic flux-return iron plates, allow for the identification of K_L^0
72 mesons and muons. The subdetectors most relevant for our study are the VXD, CDC, and
73 ECL.

74 We use collision data collected at a center-of-mass (CM) energy near the $\Upsilon(4S)$ resonance,
75 corresponding to an integrated luminosity of 189.8 fb^{-1} . We use large samples of simulated
76 $e^+e^- \rightarrow q\bar{q}$ ($q = u, d, s, c$), $\Upsilon(4S) \rightarrow B^0\bar{B}^0$ and B^+B^- events to optimize the event selection
77 and study possible background contributions. We also use simulated signal events to deter-
78 mine signal models and estimate the selection efficiency. Decays of B -mesons are simulated
79 using the EVTGEN generator [10], with the effect of final-state radiation incorporated via
80 the PHOTOS package [11]. The simulation of $e^+e^- \rightarrow q\bar{q}$ continuum background uses the
81 KKMC generator [12] interfaced to PYTHIA [13]. The interactions of final-state particles
82 with the detector are simulated using GEANT4 [14].

83 3. RECONSTRUCTION AND SELECTION

84 Tracks are reconstructed with the VXD and CDC. Photons are identified as isolated
85 energy clusters in the ECL that are not matched to any track. Candidate K_S^0 mesons are
86 reconstructed from pairs of oppositely-charged particles with dipion mass between 482 and
87 $513 \text{ MeV}/c^2$. We reconstruct π^0 candidates from pairs of photons that have energies greater
88 than 80 (223) MeV if detected in the barrel (endcap) ECL. We apply the different energy
89 thresholds to suppress beam background, which is higher in the endcap compared to barrel
90 region. The selection also requires the diphoton mass to lie between 119 and $150 \text{ MeV}/c^2$
91 and the absolute cosine of its helicity angle (i.e. the angle between a photon and the B
92 meson in the π^0 rest frame) to be less than 0.953. These criteria suppress contributions
93 from misreconstructed π^0 candidates.

94 The B -meson candidate is reconstructed by combining a K_S^0 with a π^0 candidate. For

95 this purpose, we use two kinematic variables, the beam-energy-constrained mass (M_{bc}) and
 96 the energy difference (ΔE),

$$\begin{aligned} M_{\text{bc}} &= \sqrt{E_{\text{beam}}^2 - \vec{p}_B^2}, \\ \Delta E &= E_B - E_{\text{beam}}, \end{aligned} \quad (3)$$

97 where E_{beam} is the beam energy, and E_B and \vec{p}_B are respectively the reconstructed energy
 98 and momentum of the B meson; all calculated in the CM frame.

99 The presence of a high momentum π^0 causes a correlation between M_{bc} and ΔE due
 100 to the shower leakage of final-state photons. To reduce the correlation with ΔE , we use
 101 a modified version of M_{bc} that is defined in terms of the beam energy and momenta of
 102 final-state particles as

$$M'_{\text{bc}} = \sqrt{E_{\text{beam}}^2 - \left(\vec{p}_{K_S^0} + \frac{\vec{p}_{\pi^0}}{|\vec{p}_{\pi^0}|} \sqrt{(E_{\text{beam}} - E_{K_S^0})^2 - m_{\pi^0}^2} \right)^2}, \quad (4)$$

103 where all kinematic quantities are again calculated in the CM frame. We retain candidate
 104 events satisfying $5.24 < M'_{\text{bc}} < 5.29$ GeV/ c^2 and $|\Delta E| < 0.30$ GeV.

105 To measure the proper-time difference Δt , we determine the signal and tag-side B de-
 106 cay vertices. The signal B vertex is obtained by projecting the flight direction of the K_S^0
 107 candidate back to the interaction region. The K_S^0 flight direction is determined from its
 108 decay vertex and momentum. The intersection of the K_S^0 -flight projection with the inter-
 109 action region provides a good approximation of the signal B decay vertex, since both the
 110 transverse flight length of the B^0 meson and the transverse size of the interaction region
 111 are small compared to the B^0 flight length along the boost direction. The tag-side vertex
 112 is obtained with tracks that are not associated to the $B^0 \rightarrow K_S^0 \pi^0$ decay. We obtain Δt by
 113 dividing the longitudinal distance between the signal and tag vertices by the speed of light
 114 and the Lorentz boost of the $\Upsilon(4S)$ system in the lab frame. Signal candidates with poorly
 115 measured Δt , mainly due to K_S^0 mesons decaying outside of the VXD acceptance, are sup-
 116 pressed by requiring the estimated uncertainty on Δt to be below 2.5 ps. This requirement
 117 removes about 50% of the signal candidates, which contribute negligible information to the
 118 measurement of \mathcal{A}_{CP} .

119 Events from continuum $e^+e^- \rightarrow q\bar{q}$ production are suppressed using a boosted-decision-
 120 tree (BDT) classifier [15] that exploits several event-topology variables known to provide
 121 discrimination between B -meson signal and continuum background. The following variables
 122 are those offering most discrimination between signal and continuum: modified Fox-Wolfram
 123 moments [16], CLEO cones [17], the magnitude of the thrust axis for the reconstructed B
 124 candidate and the cosine of the angle between the thrust axis of the signal B and that of
 125 rest of event. The BDT is trained on samples of simulated $e^+e^- \rightarrow q\bar{q}$, $B^0\bar{B}^0$ and B^+B^-
 126 events, each equivalent to an integrated luminosity of 1 ab^{-1} . The BDT output distribution
 127 (C_{out}) is shown in Fig. 1. We apply the criterion $C_{\text{out}} > 0.60$, which rejects about 89% of
 128 the continuum background with a 18% relative loss in signal efficiency. We translate C_{out}
 129 into a new variable,

$$C'_{\text{out}} = \ln \left(\frac{C_{\text{out}} - C_{\text{out,min}}}{C_{\text{out,max}} - C_{\text{out}}} \right), \quad (5)$$

130 where $C_{\text{out,min}} = 0.60$ and $C_{\text{out,max}} = 0.99$. The distributions of C'_{out} can be parametrized
 131 with Gaussian functions. After applying all selection criteria, the average number of B

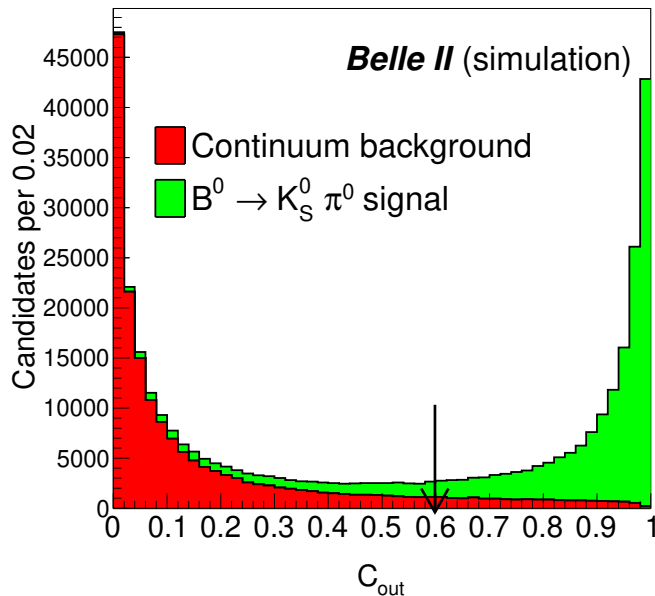


FIG. 1. Distributions of the BDT output C_{out} for simulated signal and $e^+e^- \rightarrow q\bar{q}$ events. The downward arrow indicates the position of the C_{out} selection.

133 candidates per event is 1.009. Multiple candidates arise due to a random combination of
 134 final-state particles. To select the best one in an event with multiple candidates, we first
 135 compare the π^0 mass-constrained fit χ^2 probability ('p-value'). If there are two or more B
 136 candidates sharing the same π^0 , we choose the one with the best p-value of the fit of the K_S^0
 137 vertex. This selection retains the correct B candidate in 74% of our simulated events.

138 The signal efficiency (ϵ) of correctly reconstructed events after all selection criteria have
 139 been applied is 12.3%. From simulation we find that signal candidates can be incorrectly
 140 reconstructed in 1.5% of the times by accidentally selecting a particle from the other B
 141 meson decay. We consider those candidates as part of the signal.

142 We determine the flavor of the tag-side B meson (q) from properties of final-state particles
 143 that are not associated with the reconstructed $B^0 \rightarrow K_S^0 \pi^0$ decay. The Belle II flavor tagging
 144 algorithm [18] returns, as the tagging decision, q and the tagging dilution, r , that ranges from
 145 0 (no flavor discrimination) to 1 (unambiguous flavor assignment). The multivariate flavor-
 146 tagger algorithm uses the information of B -decay products to determine the quark-flavor of
 147 B mesons.

148 4. DETERMINATION OF BRANCHING FRACTION AND CP ASYMMETRY

149 We obtain the signal yield and CP asymmetry from a four-dimensional extended
 150 maximum-likelihood fit to the unbinned distributions of M'_{bc} , ΔE , C'_{out} , and Δt . For
 151 the signal component, M'_{bc} is modeled with the sum of a Crystal Ball [19] and a Gaussian
 152 function with a common mean; ΔE with the sum of a Crystal Ball and a double Gaussian
 153 function, all three with a common mean; and C'_{out} with the sum of an asymmetric and a

154 regular Gaussian function. The signal Δt probability density function (PDF) is given by

$$\mathcal{P}_{\text{sig}}(\Delta t, q) = \frac{e^{-|\Delta t|/\tau_{B^0}}}{4\tau_{B^0}} [\{1 - q\Delta w_r + q\mu_r(1 - 2w_r)\} + \{q(1 - 2w_r) + \mu_r(1 - q\Delta w_r)\}] \quad (6)$$

$$\{\mathcal{A}_{CP} \cos(\Delta m_d \Delta t) + \mathcal{S}_{CP} \sin(\Delta m_d \Delta t)\} \otimes \mathcal{R}_{\text{sig}},$$

155 where w_r is the fraction of incorrectly tagged events, Δw_r is the difference in w_r between B^0
 156 and \bar{B}^0 , μ_r is the difference in their tagging efficiency (The tagging efficiency is the fraction
 157 of signal candidates to which a flavor tag can be assigned.), and \mathcal{R}_{sig} is the Δt resolution
 158 function. The function \mathcal{R}_{sig} is composed of two Gaussians with combined RMS of ≈ 0.9
 159 ps, and its parameters are determined with simulated events. We set τ_{B^0} to 1.520 ps, Δm_d
 160 to 0.507 ps^{-1} , and \mathcal{S}_{CP} to 0.57 [7]. The data are divided into seven $q \cdot r$ bins with the
 161 tagging parameters for each bin (w_r , Δw_r , and μ_r) fixed to the respective values obtained
 162 in Ref. [18]. The effective tagging efficiency ($\epsilon_{\text{eff}} = \sum_r \epsilon_r \cdot (1 - 2w_r)^2$, where ϵ_r is the partial
 163 effective efficiency in the r -th bin.), w_r and μ_r are $(30.0 \pm 1.2)\%$, $(2-47)\%$ and $(0.5-11)\%$,
 164 respectively. All signal PDF shapes are fixed to the values determined from a $q \cdot r$ binned
 165 fit to simulated signal events.

166 For the continuum background component, an ARGUS function [20] is used for M'_{bc} , a
 167 linear function for ΔE , and the sum of an asymmetric and a regular Gaussian function for
 168 C'_{out} . Its Δt distribution is modeled with an exponential function convolved with a Gaussian
 169 for the tail; we use a double Gaussian for its resolution function ($\mathcal{R}_{q\bar{q}}$). For the continuum
 170 background component, we float the PDF shape parameters, which are found to be common
 171 for all $q \cdot r$ bins. For the $B\bar{B}$ background component, a two-dimensional Kernel estimation
 172 PDF [21] is used to model the ΔE vs. M'_{bc} distribution, and the sum of an asymmetric
 173 and a regular Gaussian function is used for C'_{out} . Its Δt distribution is modeled with an
 174 exponential function convolved with a Gaussian for the tail; we again use a double Gaussian
 175 for its resolution function ($\mathcal{R}_{B\bar{B}}$). The $B\bar{B}$ background shape parameters are fixed from a
 176 fit to the corresponding simulated sample.

177 The fit parameters are the signal yield N_{sig} ; \mathcal{A}_{CP} , $B\bar{B}$ background yield, which is Gaussian
 178 constrained to the result of a fit to the ΔE sideband in data; continuum background yield;
 179 M'_{bc} ARGUS parameter; ΔE slope; and C'_{out} relative width for the $q\bar{q}$ component. We
 180 correct the signal M'_{bc} , ΔE , and C'_{out} PDF shapes for possible data–simulation differences,
 181 according to the values obtained with a control sample of $B^+ \rightarrow \bar{D}^0 (\rightarrow K^+ \pi^- \pi^0) \pi^+$ (charge
 182 conjugated modes are implicitly included hereafter). In order to mimic the signal decay, we
 183 use a similar π^0 selection. We use a maximum-likelihood fit to the unbinned distribution of
 184 M'_{bc} , ΔE , and C'_{out} , using PDF shapes similar to that employed in the fit to signal data.
 185 We use a control sample of $B^0 \rightarrow J/\psi (\rightarrow \mu^+ \mu^-) K_S^0$ decays to validate the time-dependent
 186 analysis. To mimic the signal decay, we do not use the two muons coming from the J/ψ
 187 decay to reconstruct the signal B decay vertex. We use a maximum-likelihood fit to the
 188 unbinned distributions of M_{bc} and Δt , using PDF shapes and resolution functions similar
 189 to those employed in the fit to signal data. The B^0 lifetime and \mathcal{A}_{CP} are measured to be
 190 $1.59^{+0.09}_{-0.08}$ ps and -0.03 ± 0.10 , respectively, which are consistent with their known values [7].
 191 This provides convincing data-driven support to the time-dependent part of the analysis.
 192 The same sample is also used to correct the Δt PDF shape parameters for possible data–
 193 simulation differences. The estimator properties (bias, uncertainty) have been thoroughly
 194 studied in simplified and realistic simulated experiments and found to be as expected.

195 Figure 2 shows the four projections of the fit to the seven $q \cdot r$ -integrated data samples.
 196 For each projection the signal enhancing criteria, $5.27 < M'_{\text{bc}} < 5.29 \text{ GeV}/c^2$, $-0.15 < \Delta E <$

197 0.10 GeV, $|\Delta t| < 10.0$ ps, and $C'_{\text{out}} > 0.0$, are applied except for the variable displayed. The
 198 obtained signal yield is 135^{+16}_{-15} , where the quoted uncertainty is statistical only. We also find
 199 2214^{+49}_{-48} continuum and 44 ± 5 $B\bar{B}$ background events. We determine the branching fraction
 200 using the following formula:

$$\mathcal{B}(B^0 \rightarrow K^0 \pi^0) = \frac{N_{\text{sig}}}{2 \times N_{B\bar{B}} \times f^{00} \times \epsilon \times \mathcal{B}_s}, \quad (7)$$

201 where $N_{B\bar{B}} = (197.2 \pm 5.70) \times 10^6$, $f^{00} = 0.487 \pm 0.010$ [22], and $\mathcal{B}_s = 0.5$ are the number
 202 of $B\bar{B}$ pairs, $\Upsilon(4S) \rightarrow B^0 \bar{B}^0$ branching fraction, and $K^0 \rightarrow K_s^0$ branching fraction, respec-
 203 tively. The $B^0 \rightarrow K^0 \pi^0$ branching fraction and direct CP asymmetry (\mathcal{A}_{CP}) are measured
 204 to be $(11.0 \pm 1.2 \pm 1.0) \times 10^{-6}$ and $0.41^{+0.30}_{-0.32} \pm 0.08$, respectively. The first uncertainties are
 205 statistical and the second are systematic (described in Section 5). This extends the previous
 206 measurement [23] of \mathcal{B} and \mathcal{A}_{CP} in $B^0 \rightarrow K^0 \pi^0$ decays, where no information on the proper
 207 time difference was used.

208 5. SYSTEMATIC UNCERTAINTIES

209 Various systematic uncertainties contributing to \mathcal{B} and \mathcal{A}_{CP} are listed in Table I. Assum-
 210 ing these sources to be independent, we add their contributions in quadrature to obtain the
 211 total systematic uncertainty. The systematic uncertainty due to possible differences between
 212 data and simulation in the reconstruction of charged particles is 0.3% per track [24]. We
 213 linearly add this uncertainty in $mathcal{B}$ for each of the two pion tracks coming from the
 214 decay of the K_s^0 of the signal B . From a comparison of the K_s^0 yield in data and simulation,
 215 we find that the ratio of the K_s^0 reconstruction efficiency changes approximately linearly as a
 216 function of its flight length [24]. We apply an uncertainty of 0.4% for each centimeter of the
 217 average flight length of the K_s^0 candidates resulting in a 4.2% total systematic uncertainty
 218 in \mathcal{B} . We estimate the systematic uncertainty due to possible differences between data and
 219 simulation in the π^0 reconstruction and selection by comparing the inclusive decay sample of
 220 $D^0 \rightarrow K^- \pi^+ \pi^0$ with $D^0 \rightarrow K^- \pi^+$ [25]. The data–simulation efficiency ratio is found to be
 221 close to unity with an uncertainty of 7.5%, which we assign as the systematic uncertainty in
 222 \mathcal{B} . We evaluate possible data–simulation differences in the continuum-suppression efficiency
 223 using the control sample of $B^+ \rightarrow \bar{D}^0 (\rightarrow K^+ \pi^- \pi^0) \pi^+$. As the ratio of efficiencies obtained
 224 in data and simulation is close to unity, the statistical uncertainty on the ratio (1.6%) is
 225 assigned as a systematic uncertainty to \mathcal{B} . We estimate the systematic uncertainty in \mathcal{A}_{CP}
 226 due to the uncertainty in the wrong tag fraction by varying the parameter individually for
 227 each $q \cdot r$ region by its 1σ uncertainty. The systematic uncertainty due to the Δt resolution
 228 function is estimated in a similar fashion. As external inputs τ_{B^0} , Δm_d , and \mathcal{S}_{CP} are fixed
 229 to their known values in the fit, the associated systematic uncertainties are estimated by
 230 varying their values by $\pm 1\sigma$. In the nominal fit, we assume the $B\bar{B}$ -background decays to
 231 be CP symmetric. To account for a potential CP asymmetry in the $B\bar{B}$ -background, we use
 232 an alternative Δt PDF given by

$$\mathcal{P}_{B\bar{B}}(\Delta t, q) = \frac{e^{-|\Delta t|/\tau_{B^0}}}{4\tau_{B^0}} [1 + q\{\mathcal{A}'_{CP} \cos(\Delta m_d \Delta t) + \mathcal{S}'_{CP} \sin(\Delta m_d \Delta t)\}] \otimes R_{B\bar{B}}. \quad (8)$$

233 We perform simplified simulated experiments fits by varying \mathcal{S}'_{CP} and \mathcal{A}'_{CP} from +1 to -1.
 234 We then calculate the deviations in signal \mathcal{A}_{CP} from its nominal value. These deviations are

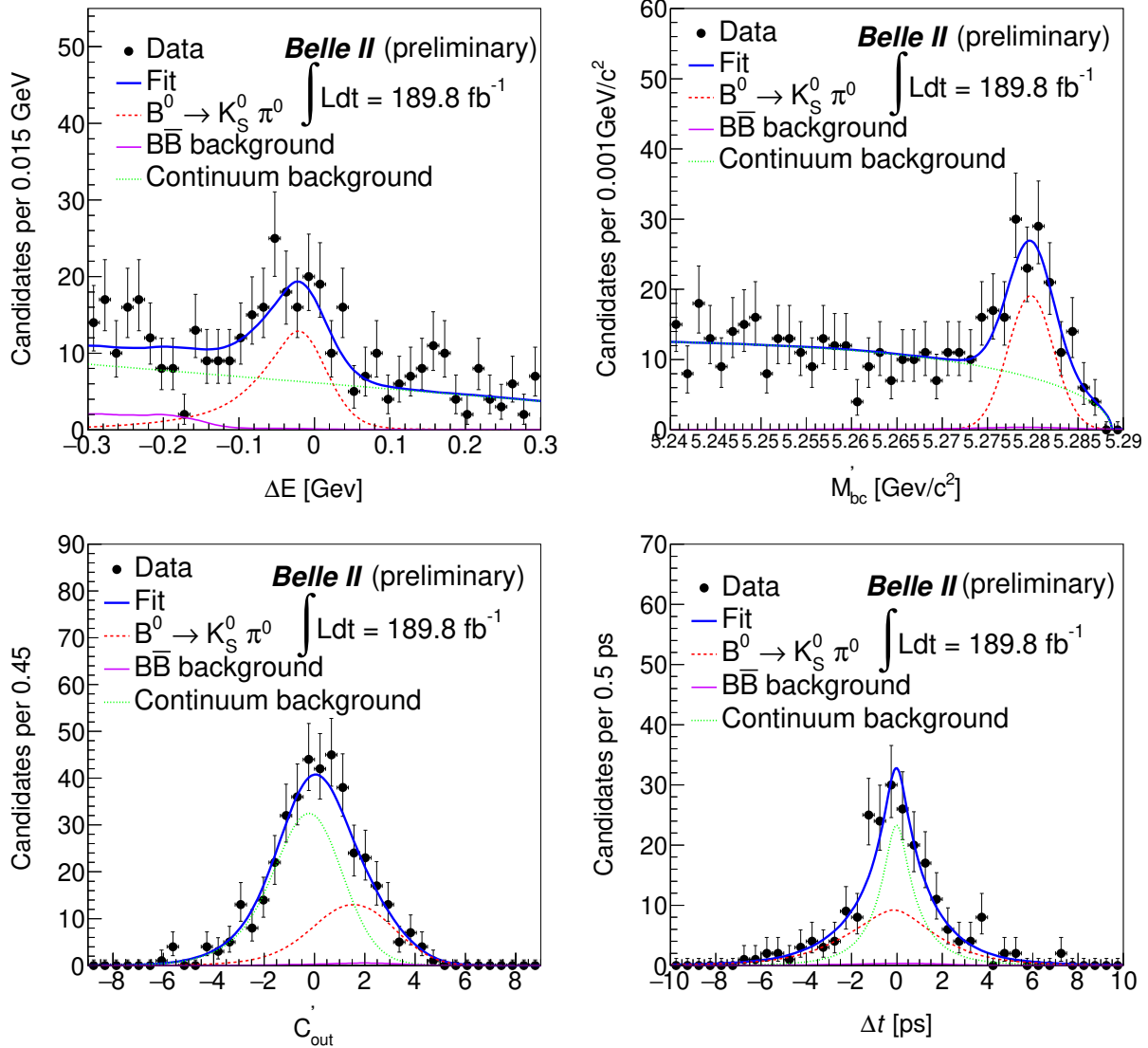


FIG. 2. Signal enhanced fit projections of ΔE (top-left), M'_{bc} (top-right), C'_{out} (bottom-left), and Δt (bottom-right) shown for the sample integrated in the seven $q \cdot r$ bins.

235 assigned as a systematic uncertainty to \mathcal{A}_{CP} due to the asymmetry of the $B\bar{B}$ background.
 236 An overall uncertainty of 3.2% in \mathcal{B} is taken as a systematic uncertainty due to the number
 237 of $B\bar{B}$ pairs used, which includes the uncertainty in f^{00} , cross section, integrated luminosity,
 238 and possible shifts from the peak CM energy as a function of time. The uncertainties due to
 239 the signal PDF shape parameters are estimated by varying their correction factors by $\pm 1\sigma$,
 240 where σ denotes the corresponding statistical uncertainties. Similarly, the uncertainties
 241 due to the background PDF shape are calculated by varying all fixed parameters by $\pm 1\sigma$,
 242 determined from the fit to simulated samples. We fix the M'_{bc} ARGUS endpoint to the value
 243 obtained from a fit to the ΔE sideband data. Subsequently we vary it by $\pm 1\sigma$ to assign a
 244 systematic uncertainty, where σ is the uncertainty from the fit. A potential fit bias is checked
 245 by performing an ensemble test comprising 1000 simplified simulated experiments in which
 246 signal events are drawn from the corresponding simulation sample and background events

247 are generated according to their PDF shapes. We calculate the mean shift of signal yield
 248 from the input value and assign it as a systematic uncertainty. The tag-side interference is
 249 arise due to the interference between CKM-favored and CKM-supressed in tree level decay.
 250 The systematic uncertainty in \mathcal{A}_{CP} assigned to tag-side interference is taken from Ref. [6].
 251 A possible systematic uncertainty related to VXD misalignment is neglected in this study.

TABLE I. List of systematic uncertainties contributing to the branching fraction and direct CP asymmetry.

Source	$\delta\mathcal{B}$ (%)	$\delta\mathcal{A}_{CP}$
Tracking efficiency	0.6	–
K_S^0 reconstruction efficiency	4.2	–
π^0 reconstruction efficiency	7.5	–
Continuum suppression efficiency	1.6	–
Number of $B\bar{B}$ pairs	3.2	–
Flavor tagging	–	0.040
Resolution function	–	0.050
External inputs	0.4	0.021
$B\bar{B}$ background asymmetry	–	0.002
Signal modelling	1.0	0.015
Background modelling	0.9	0.004
Possible fit bias	2.0	0.010
Tag-side interference	–	0.038
Total	9.6	0.086

252 6. SUMMARY

253 We report measurements of the branching fraction and direct CP asymmetry in $B^0 \rightarrow$
 254 $K^0\pi^0$ decays using a data sample, corresponding to 189.8fb^{-1} of integrated luminosity,
 255 recorded by Belle II at the $\Upsilon(4S)$ resonance. The observed signal yield is 135^{+16}_{-15} . We measure
 256 $\mathcal{B}(B^0 \rightarrow K^0\pi^0) = [11.0 \pm 1.2(\text{stat}) \pm 1.0(\text{syst})] \times 10^{-6}$ and $\mathcal{A}_{CP} = -0.41^{+0.30}_{-0.32}(\text{stat}) \pm 0.08(\text{syst})$.
 257 This is the first measurement of \mathcal{A}_{CP} in $B^0 \rightarrow K^0\pi^0$ performed at Belle II using a decay-
 258 time-dependent analysis. The results agree with previous determinations [7, 23].

259 7. ACKNOWLEDGEMENT

260 We thank the SuperKEKB group for the excellent operation of the accelerator; the KEK
 261 cryogenics group for the efficient operation of the solenoid; and the KEK computer group
 262 for on-site computing support.

263 [1] M. Fujikawa et al. (Belle Collaboration), Phys. Rev. D **81**, 011101 (2010).

- 264 [2] B. Aubert et al. (BaBar Collaboration), Phys. Rev. D. **79**, 052003 (2009).
265 [3] M. Gronau, Phys. Lett. B **627**, 82 (2005).
266 [4] T. Gershon and A. Soni, J. Phys. G **33** (2007) 479–492.
267 [5] P. A. Zyla et al., Particle Data Group, Review of Particle Physics, PTEP **2020**, 083C01 (2020)
268 [6] I. Adachi et al. (Belle Collaboration), Phys. Rev. Lett. **108**, 171802 (2012).
269 [7] Y. Amhis et al. (Heavy Flavor Averaging Group), Eur. Phys. J. C **81**, 226 (2021),
270 arXiv:1909.12524.
271 [8] T. Abe et al. (Belle II Collaboration), KEK Report 2010-1, arXiv:1011.0352.
272 [9] K. Akai, K. Furukawa, and H. Koiso (SuperKEKB Group), Nucl. Instrum. Meth. A **907**, 188
273 (2018).
274 [10] D. Lange, Nucl. Instrum. Meth. A **462**, 152 (2001).
275 [11] E. Barberio, B. van Eijk, and Z. Was, Comp. Phys. Comm. **66**, 115 (1991).
276 [12] B. Ward, S. Jadach, and Z. Was, Nucl. Phys. B Proc. Suppl. **116**, 73 (2003)
277 [13] T. Sjöstrand, S. Mrenna, and P. Skands, Comp. Phys. Comm. **178**, 852 (2008).
278 [14] S. Agostinelli et al. (GEANT4 Collaboration), Nucl. Instrum. Meth. A **506**, 250 (2003).
279 [15] T. Keck, arXiv:1609.06119.
280 [16] G. C. Fox and S. Wolfram, Phys. Rev. Lett. **41**, 1581 (1978).
281 [17] D. M. Asner et al. (CLEO Collaboration), Phys. Rev. D **53**, 1039 (1996).
282 [18] F. Abudinén et al. (Belle II Collaboration), Eur. Phys. J. C **82**, 283 (2022).
283 [19] T. Skwarnicki, PhD thesis, INP Krakow, DESY-F31-86-02 (1986).
284 [20] H. Albrecht et al. (ARGUS Collaboration), Phys. Lett. B **241**, 278 (1990).
285 [21] K. S. Cranmer, Comp. Phys. Comm. **136**, 198 (2001).
286 [22] B. Aubert et al. (BaBar Collaboration), Phys. Rev. Lett. **95** (2005) 042001.
287 [23] F. Abudinén et al. (Belle II Collaboration), BELLE2-CONF-PH-2021-001, arXiv:2104.14871.
288 [24] V. Bertacchi et al. (Belle II Tracking Group), Comp. Phys. Comm. **259**, 107610 (2021).
289 [25] G. Bonvicini et al. (CLEO Collaboration), Phys. Rev. D **89**, 072002 (2014).
290 [26] L. Šantelj et al. (Belle Collaboration), JHEP **10**, 165 (2014).